Molecular and isotopic evidence reveals the end-Triassic carbon isotope excursion is not from massive exogenous light carbon

Calum P. Fox[a,b,1], Xingqian Cui[c,d,1], Jessica H. Whiteside[e,2], Paul E. Olsen[f,2], Roger E. Summons[d], and Kliti Grice[a,2]

[a]Western Australia Organic & Isotope Geochemistry Centre, School of Earth and Planetary Sciences, The Institute for Geoscience Research, Curtin University, Perth, WA 6845, Australia; [b]Department of Earth Sciences, Khalifa University of Science and Technology, Abu Dhabi, United Arab Emirates; [c]School of Oceanography, Shanghai Jiao Tong University, 200030 Shanghai, China; [d]Department of Earth, Atmospheric and Planetary Sciences, Massachusetts Institute of Technology, Cambridge, MA 02139; [e]Ocean and Earth Science, National Oceanography Centre Southampton, University of Southampton, SO14 3ZH Southampton, United Kingdom; and [f]Department of Earth and Environmental Sciences, Lamont-Doherty Earth Observatory of Columbia University, Palisades, NY 10964

Contributed by Paul E. Olsen, October 8, 2020 (sent for review October 9, 2019; reviewed by Simon C. George and Jennifer C. McElwain)

The negative organic carbon isotope excursion (CIE) associated with the end-Triassic mass extinction (ETE) is conventionally interpreted as the result of a massive flux of isotopically light carbon from exogenous sources into the atmosphere (e.g., thermogenic methane and/or methane clathrate dissociation linked to the Central Atlantic Magmatic Province [CAMP]). Instead, we demonstrate that at its type locality in the Bristol Channel Basin (UK), the CIE was caused by a marine to nonmarine transition resulting from an abrupt relative sea level drop. Our biomarker and compound-specific carbon isotopic data show that the emergence of microbial mats, influenced by an influx of fresh to brackish water, provided isotopically light carbon to both organic and inorganic carbon pools in centimeter-scale water depths, leading to the negative CIE. Thus, the iconic CIE and the disappearance of marine biota at the type locality are the result of local environmental change and do not mark either the global extinction event or input of exogenous light carbon into the atmosphere. Instead, the main extinction phase occurs slightly later in marine strata, where it is coeval with terrestrial extinctions and ocean acidification driven by CAMP-induced increases in Pco_2; these effects should not be conflated with the CIE. An abrupt sea-level fall observed in the Central European basins reflects the tectonic consequences of the initial CAMP emplacement, with broad implications for all extinction events related to large igneous provinces.

large igneous provinces | carbon isotopes | end-Triassic mass extinction | biomarkers

Most of the major mass extinctions of the last 300 My, as well as some of the lesser biotic turnover events, are associated with reorganizations or perturbations of the Earth's carbon cycle, caused at least, in part, by massive inputs of carbon either sourced from or triggered by the emplacement of huge flood basalt-dominated igneous provinces (1). The most aerially extensive of these magmatic systems, the Central Atlantic Magmatic Province (CAMP), has been tied (on land) by high-resolution geochronology to the end-Triassic mass extinction (ETE) event at 201.6 Ma (2, 3). In marine environments, the unequivocal link between the ETE and the CAMP is far less direct, but the prevailing view is that the profound negative (>5‰ depletion in $\delta^{13}C$) carbon isotopic excursion (CIE) associated with the ETE was caused by a massive input of exogenous, isotopically light carbon to the ocean–atmosphere system from thermogenic and/or methane clathrate source(s), triggered by the initial phase of the CAMP. This dramatic CIE is often referred to as the "initial" CIE but herein, to avoid confusion, is named as the Bristol Channel Basin (BCB) CIE, reflecting the area where this CIE was first observed (4). In order to constrain the source and timing of the end-Triassic isotopic shifts and to deconvolve this $\delta^{13}C_{org}$ excursion, we utilized organic biomarker and compound-specific isotopic techniques at one of the most extensively studied areas of the ETE, the BCB of southwestern (SW) United Kingdom (Fig. 1). Our results indicate that the BCB CIE was a consequence of environmentally driven ecosystem changes in carbon sources due to regional sea-level change, not the input of exogenous light carbon. Furthermore, the data suggest that the marine ETE occurred after this pronounced isotopic shift, in the latest Rhaetian, when massive inputs of CAMP-derived CO_2 caused ocean acidification, related environmental disruptions, and true global marine extinction. Consequently, the terminal Triassic CIE, although it may chronicle the initiation of the CAMP, is not directly associated with the ETE.

Geological and Environmental Context

The BCB is a subdivision of the 1.8 million square-kilometer early Mesozoic Pangean Central European Basin. This basin was largely continental in the Norian (228 to 205.7 Ma) but, by Rhaetian time in the Late Triassic (205.7 to 201.4 Ma), became

Significance

The end-Triassic mass extinction that occurred ~202 Ma is one of the "Big Five" biotic crises of the Phanerozoic Eon. It is also accompanied by an organic carbon isotopic excursion that has long been interpreted as the result of a global-scale carbon-cycle disruption. Rather than being due to massive inputs of exogenous light carbon into the ocean–atmosphere system, the isotopic excursion is shown here to reflect regional sea-level change that caused a transition from a marine ecosystem to a less saline, shallow-water, microbial-mat environment and resultant changes in the sources of organic matter. The mass extinction that occurred slightly later, caused by abrupt injection of volcanogenic CO_2, is accompanied by only modest changes in organic carbon isotopic composition.

Author contributions: C.P.F., J.H.W., P.E.O., and K.G. designed research; C.P.F., X.C., J.H.W., P.E.O., R.E.S., and K.G. performed research; C.P.F., X.C., J.H.W., P.E.O., R.E.S., and K.G. analyzed data; and C.P.F., X.C., J.H.W., P.E.O., R.E.S., and K.G. wrote the paper.

Reviewers: S.C.G., Macquarie University; and J.C.M., Trinity College Dublin.

The authors declare no competing interest.

Published under the PNAS license.

[1]C.P.F. and X.C. contributed equally to this work.

[2]To whom correspondence may be addressed. Email: J.Whiteside@soton.ac.uk, polsen@ldeo.columbia.edu, or K.grice@curtin.edu.au.

This article contains supporting information online at https://www.pnas.org/lookup/suppl/doi:10.1073/pnas.1917661117/-/DCSupplemental.

First published November 16, 2020.

Downloaded at Columbia Univ Lib on January 14, 2021

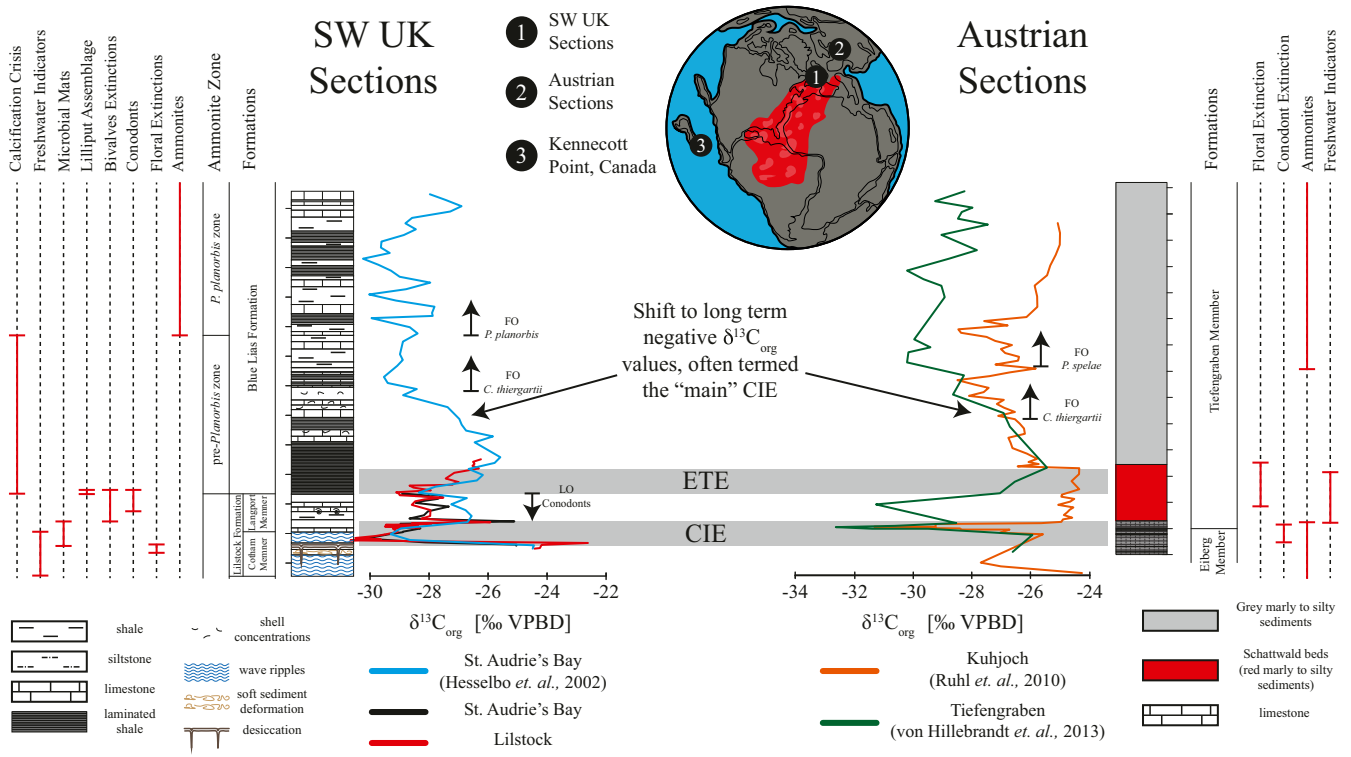

Fig. 1. Critical events around the ETE in the BCB (St. Audrie's Bay and Lilstock) and Austrian (Kuhjoch and Tiefengraben) areas. St. Audrie's Bay and Lilstock $\delta^{13}C_{org}$ data from the current study are displayed in black and red, respectively. St. Audrie's Bay lithostratigraphy and extended $\delta^{13}C_{org}$ data (blue) are from ref. 4. Austrian lithostratigraphy and Kuhjoch $\delta^{13}C_{org}$ data (orange) are from ref. 5, and Tiefengraben $\delta^{13}C_{org}$ data (green) are from ref. 6. SW UK freshwater indicators are from refs. 7–9; bivalve extinctions are from refs. 10 and 11; conodont extinctions are from ref. 12; and floral extinctions are from ref. 13. Austrian floral extinctions, conodont extinctions, ammonites, and freshwater indicators are from ref. 6. Note that the order of conodont and floral changes are reversed at the two areas, requiring the actual extinctions to occur simultaneously and later, as shown by the ETE label. Ticks are at 1-m intervals. Pangea reconstruction is based on ref. 4, including the lateral extent of CAMP (red). FO, first occurrence; LO, last occurrence; VPBD, Vienna Pee Dee Belemnite.

an epicontinental sea with restricted circulation. Based on lithology and fossil evidence in the Westbury and Lilstock formations, the northern parts of this seaway (including the United Kingdom) had fluctuating salinity (14). Located on the northern flank of the CAMP (Fig. 1), the Central European Basin contains no lava flows or ash beds, hindering direct correlation with paroxysmal magmatic events. A well-documented cycle of sea-level fall and then rise throughout the basin occurred in the few hundred thousand years of the latest Rhaetian (15). It is within this environmental context that the BCB CIE, and its more southern correlatives, formed close in time to the ETE and initiation of the CAMP.

Results and Discussion

Sea-Level Fall Resulted in Microbial Mat Emergence and Ecological Stress. Biomarker data for both the St. Audrie's Bay and Lilstock sections of the BCB (*SI Appendix*, Fig. S1) suggest that the BCB CIE is a feature driven by ecological community changes forced by decreasing water depth and salinity within the basin and, by extension, to the European basin as a whole. We describe the biomarker results in stratigraphic (i.e., chronological) order as follows.

After an extended interval of predominantly nonmarine redbed deposition spanning most of the Triassic, the BCB was flooded by marine waters of abnormally low salinity, which deposited the dark mudstones of the Westbury Formation in the Rhaetian (14). Both sections show a relatively abrupt upward transition to the lighter-colored lower Cotham Member of the Lilstock Formation, characterized by fewer marine fossils and abundant oscillation ripples, indicating a shallowing water depth but without much change in faunal composition. The lower Cotham and uppermost Westbury were subjected to folding and brecciation attributed, at least in part, to syndepositional megaseismic event(s) (16). Through the Westbury to Cotham lithological transition, perturbations in biomarker-inferred ecological and redox conditions are apparent. C_{30} steranes (24-*n*-propyl cholestanes), compounds derived from marine pelagophyte algae, show a constant decrease to zero (Fig. 2). Except for low-diversity marine bivalves identified in the lower part of the Cotham Member in Lavernock Point, South Wales, a near absence in marine fossils throughout the Cotham Member supports a transition from a residual sea to a restricted shallowing nonmarine environment (7, 17). Furthermore, declining values of the gammacerane index and ratios of isorenieratane/triaromatic steroids signify the termination of stratification (18) and disappearance of photic zone euxinia (a condition in which hydrogen sulfide is present in the sun-lit region of the water column) (19–22), respectively (Fig. 2). This is likely caused by the strong mixing of shallowing water that recharges oxygen throughout the water column. Additionally, strong shifts in the relative abundances of C_{27}, C_{28}, and C_{29} steranes that generally represent red, chlorophyll *c*-containing, and green algae, respectively, are observed (*SI Appendix*, Fig. S2), implying an unstable environment sensitive to ambient perturbations, a common observation associated with shallowing water.

Truncating the folded lower Cotham seismite is an erosional surface downward from which intrude deep desiccation cracks (~>1 m), at which level, the BCB CIE and the upper Cotham Member begins (Fig. 2). This sedimentological feature, as well as other evidence of desiccation with smaller crack length, wave ripples (Fig. 2), and possible rain drop imprints (7), indicates the CIE is recorded during maximum regression and centimeter-scale

Downloaded at Columbia Univ Lib on January 14, 2021

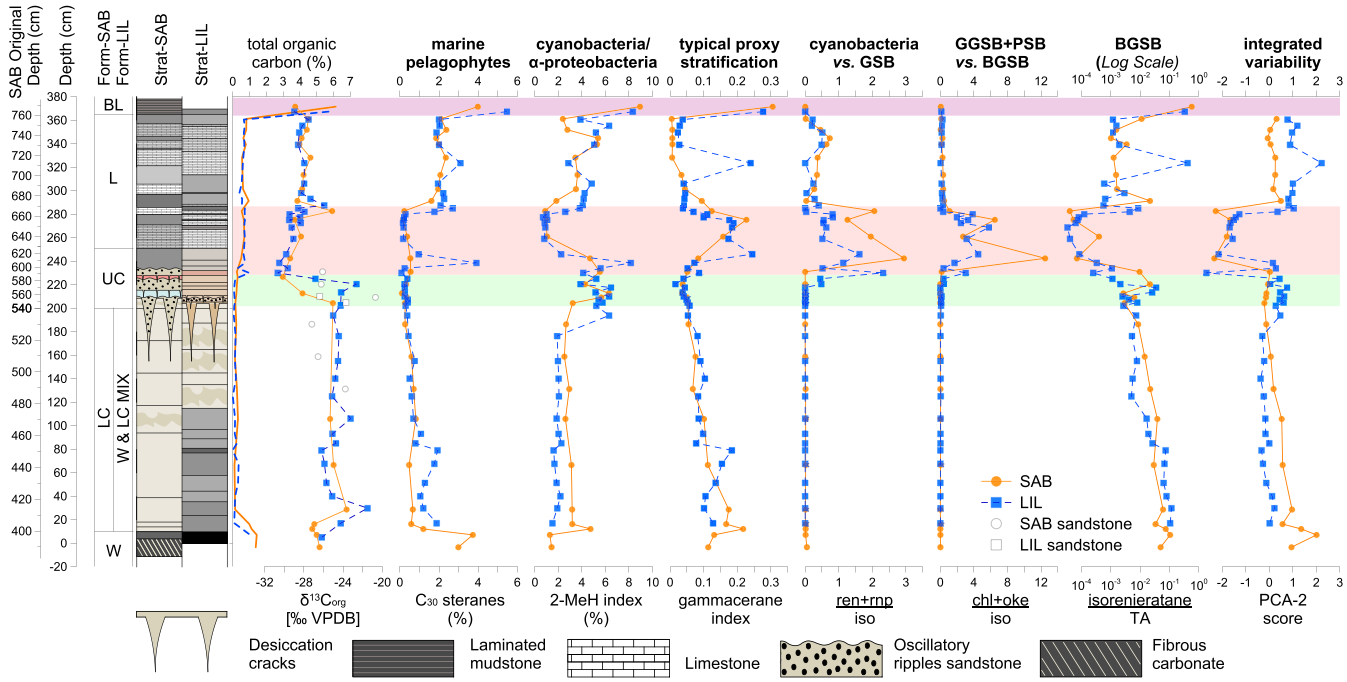

Fig. 2. Biomarker evidence of depositional facies change at St. Audrie's Bay (orange circles and solid lines) and Lilstock (blue squares and dashed lines) compared to the $\delta^{13}C_{org}$ and TOC records. The BCB CIE is displayed in light green (lower CIE) and pink (upper CIE), while newly proposed extinction onset is highlighted in light purple. The interpreted meaning of each biomarker-based proxy is indicated in bold above each column. Full details of the biomarker measurements are in *SI Appendix*. PCA loosely represents an index of integrated variability corresponding to microbial-mat formation and is represented here by PC-2. Note that PCA was carried out for all samples except two samples from Blue Lias Formation, to avoid large bias introduced by the outliers, and that the isorenieratane/triaromatic steroids are plotted in log scale. More information with regard to the comparison between PC-1 and PC-2 is available in *SI Appendix*. BGSB, low-light deep water-adapted brown-pigmented green sulfur bacteria; BL, Blue Lias Formation; chl+oke, chlorobactane plus okenane; Form, formation; GGSB, high light-adapted green-pigmented GSB; iso, isorenieratane; L, Langport Member; LC, Lower Cotham Member; LIL, Lilstock; ren, renieratane; rnp, renierapurpurane; SAB, St. Audrie's Bay; TA, triaromatic steroids; UC, Upper Cotham Member; VPBD, Vienna Pee Dee Belemnite; W, Westbury Formation.

water depth (23). These upper Cotham Member mudstones vary in color from tan and red to light gray and have C_{30} sterane index values near zero, implying freshwater recharge. Both biomarkers and $\delta^{13}C_{org}$ values in the upper Cotham Member shift in the position and magnitude within the CIE. Consequently, the CIE can be divided into two stages, the "lower CIE" and "upper CIE."

The lower CIE is characterized by large offsets in the timing and magnitude (~3 ‰) of $\delta^{13}C_{org}$ between the two sections, likely related to small differences in sedimentation rates (i.e., Lilstock encompasses the entire CIE, and St. Audrie's Bay encompasses a variety of sedimentary rock types containing the excursion). Consistently low 3-methylhopane (3-MeH) index values (*SI Appendix*, Fig. S2), which represent minimal contributions from aerobic methanotrophs, and increases in 2-methylhopane (2-MeH) index values (Fig. 2) are also observed. Although 2-MeH is typically used as a biomarker for cyanobacteria, other organisms, exemplified by α-proteobacteria, have the capacity to produce 2-methyhopanoids (23, 24), preserved as 2-MeHs in sediments, complicating interpretations of the 2-MeH index in the geological record. Rather, studies suggest that modern marine cyanobacteria are minor producers of 2-methylhopanoids compared to other sources such as α-proteobacteria and plant-associated (i.e., soil, wood degradation), terrestrial, and freshwater environments (25, 26). In the context of microbial systems, the modern Laguna Guerrero Negro (Baja California) hypersaline microbial mats and Highborne Cay stromatolites (Bahamas) show evidence of *hpnP* genes (required to produce 2-methylhopanoids) equally contributed by cyanobacteria and α-proteobacteria (25). Contrastingly, the pustular and smooth microbial mats in the hypersaline lagoon of Shark Bay, Western Australia, show evidence of *hpnP* genes from a predominantly cyanobacterial source despite a major contribution of α-proteobacteria in the mats (27). Whether primarily sourced from cyanobacteria or α-proteobacteria, increases in the 2-MeH index in the lower CIE interval most simply interpreted to constitute a microbial-mat source. Additionally, a well-mixed water column at the lower CIE is evidenced by low gammacerane index values, consistent with tan to red-colored mudstones. Chlorobactane and okenane, pigment-derived biomarkers for high light-adapted anoxygenic phototrophic green-pigmented green (GSB) and purple (PSB) sulfur bacteria (20, 28), respectively, are barely detectable (*SI Appendix*, Fig. S8). Increasing relative abundances of low light-adapted brown-pigmented GSB, indicated by ratios of isorenieratane/triaromatic steroids, are also observed (Fig. 2) (29, 30); however, such increases are mostly an order of magnitude lower compared to those above and below the CIE. Altogether, these changes strongly argue for the initiation of freshening and shallowing conditions populated by thin, microbial-mat communities containing oxygenic cyanobacteria and/or α-proteobacteria and point to the dramatic perturbations to the ecosystem and environment at the lower CIE stage.

Nearly absent C_{30} steranes in the upper CIE, except one outlier sample, corroborate the interpretation of a nonmarine environment throughout the Cotham Member. Another line of evidence is the elevated ratios of (renieratane and renierapurpurane)/isorenieratane ([ren+rnp])/iso) (Fig. 2). Renieratane and renierapurpurane are carotenoid biomarkers sourced from numerous strains of cyanobacteria (31, 32) and high (ren+rnp)/iso ratios, as observed in the upper CIE, are typical of Phanerozoic lacustrine settings with low sulfate inventories (33). Increases in chlorobactane and okenane carotenoid biomarkers suggest expansion of anoxic green-pigmented GSB and PSB layers in

Downloaded at Columbia Univ Lib on January 14, 2021

microbial mats beneath surficial cyanobacterial layer(s) (Fig. 2). The cooccurrence of all these carotenoids requires redox stratification, a niche most parsimoniously attributed to a microbial-mat source (29). Additionally, the gammacerane index increases in the upper CIE further support microbial-mat formation and/or freshwater input. Although typically used as a stratification proxy in marine or hypersaline lagoon settings (18), increases of gammacerane in the upper CIE likely result from other source(s) of tetrahymanol (i.e., gammacerane precursor), such as phototrophic bacteria (34) and/or freshwater ciliates (35). Notably, many α-proteobacteria that produce 2-methylhopanoids also have the capacity to produce tetrahymanol, and an inverse relationship is observed between these compounds (24, 36). Thus, upper CIE gammacerane index increases are interpreted to be a direct response to ecological and environmental changes different from the lower CIE. Some of the largest and most dramatic changes in the relative abundances of the predominant C_{27}, C_{28}, and C_{29} steranes and the ratio of algae to bacteria are also observed in the upper CIE at lowest $\delta^{13}C_{org}$ values (*SI Appendix*, Fig. S2). The oligotrophic and shallow water conditions of the upper Cotham Member support a habitat in which photosynthetic microbial mats could thrive alongside the observed generally oligohaline or freshwater biota (37), including darwinulid ostracodes, spinocaudatan crustaceans, and the bryophyte *Naiadita lanceolata* (7–9).

The transition from the lower CIE to the upper CIE witnessed a significant reformation of the aquatic microbial community, with the upper CIE hosting the lowest $\delta^{13}C_{org}$ values (Figs. 2 and 3). In addition, a principal component analysis (PCA) of the biomarkers interpreted to relate to a microbial-mat source during the CIE (Fig. 2) reveals that most of the variability occurs during the upper CIE and that 55 to 65% of variation can be explained in the first (PC-1) and second (PC-2) principal components (*SI Appendix*, *Supplementary Text* and Fig. S9).

The coeval Cotham Marble (covering 2,000 km^2 elsewhere in the SW United Kingdom) also contains the remains of microbial-mat habitats during the CIE. Comprised of microbialites and laminar and thrombolytic stromatolites, this unit also displays a negative carbon isotopic profile (38, 39). Similar biomarkers have been attributed to microbial mats in the Chicxulub crater core that were transported from a carbonate platform by seiches and tsunamis after an asteroid impact (40). Accompanying the upper Cotham low-stand is the replacement of the marine biota by a nonmarine flora and fauna (7, 9, 13). Although the extinction horizon is conventionally placed at this level at the CIE, the absence of marine Triassic taxa cannot be attributed to extinction because those taxa would be absent in the nonmarine BCB even if the ETE never occurred.

Return to Marine Conditions. The termination of the CIE in the lower Langport Member is accompanied by a transgressive event that led to the reestablishment of a transitional marine environment, evidenced by a rise in C_{30} steranes and a return of the diagnostic carotenoid isorenieratane as the dominant photosynthetic pigment (Fig. 2). The synchronous responses in bulk isotope, C_{30} steranes, and other proxies (discussed later) strongly argue that the termination of the CIE is related to local depositional environment shifts (Fig. 2 and *SI Appendix*, Fig. S2). For example, this boundary witnessed a rise in 2-MeH, sudden decline in freshwater ciliates and/or phototrophic bacteria (gammacerane index), elimination of aromatic carotenoid-producing cyanobacteria ([ren+rnp]/iso), resurgence of brown-pigmented GSB (isorenieratane/triaromatic steroids) (Fig. 2), and a strong methane cycle modulated by methanotrophs (3Me-H) (*SI Appendix*, Fig. S2). Additionally, minor perturbations in eukaryotic communities are observed based on $C_{27–29}$ sterane compositions (*SI Appendix*, Fig. S2). Interestingly, C_{30} steranes anticorrelate with the relative density of cyanobacteria/α-proteobacteria vs. aerobic methanotrophs (*SI Appendix*, Fig. S3), a relationship that is contrary to common observations, as summarized in ref. 41. In our case, this pattern is most reasonably explained as reflecting the demise of the freshwater nitrogen-fixing cyanobacteria and/or α-proteobacteria present in microbial mats brought about by

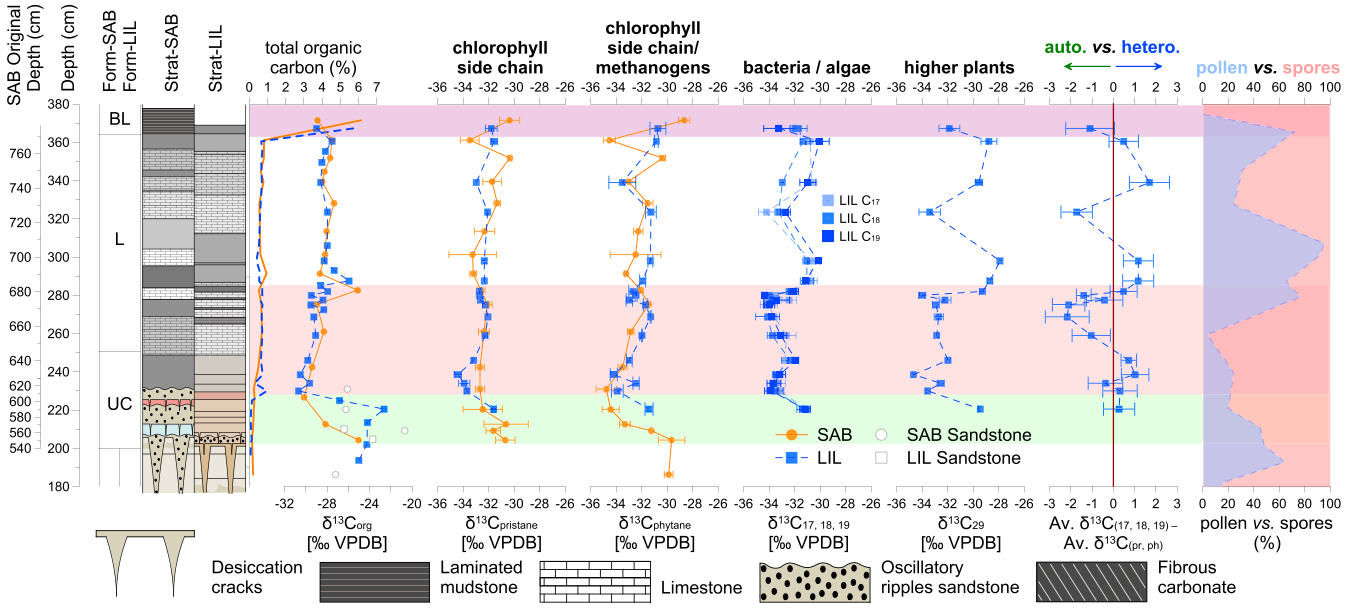

Fig. 3. Compound-specific isotope analysis of pristane and phytane from St. Audrie's Bay and Lilstock and *n*-alkanes from Lilstock. $\delta^{13}C_{17,\ 18,\ 19}$ indicates isotopic values of C_{17}, C_{18}, and C_{19} *n*-alkanes displayed in different color intensities. Av. $\delta^{13}C_{(17,\ 18,\ 19)}$–Av. $\delta^{13}C_{(pr,\ ph)}$ represents isotope mean value offsets between $C_{17,18,19}$ *n*-alkanes and pristane + phytane used to investigate autotrophy (auto.) vs. heterotrophy (hetero.). St. Audrie's Bay palynology data were previously reported in ref. 13 and are correlated here to Lilstock through lithological changes. The inferred meaning of each compound is indicated in bold above each column. BL, Blue Lias Formation; L, Langport Member; LIL, Lilstock; SAB, St. Audrie's Bay; UC, Upper Cotham Member; VPBD, Vienna Pee Dee Belemnite.

Downloaded at Columbia Univ Lib on January 14, 2021

the marine transgression. Dynamic shifts in almost all biomarkers and PCA scores are observed in one sample of the Langport Member at Lilstock without significant change in $\delta^{13}C_{org}$ composition (Fig. 2 and *SI Appendix*, Fig. S9). However, this interval is deposited within a heavily bioturbated level not observed at St. Audrie's Bay and is therefore considered a likely outlier. A shift back toward marine conditions in the middle to upper Langport Member is also indicated by a return of marine bivalve taxa, several of which disappeared at the base of the freshwater input at the CIE. Although several of these bivalve taxa persist into the overlying Blue Lias Formation, there are also several regional last appearances (10, 11). The uppermost mollusk-bearing Langport Member resembles the bioturbated marlstone and limestone facies that occur cyclically in the overlaying Blue Lias Formation, reflecting a return to fully marine conditions (Fig. 1). Conodonts occur for the first time in this unit, only to have their last occurrence in the overlying basal Blue Lias Formation (12), which also contains the last occurrence of the characteristic Late Triassic reptile clade Phytosauria (42).

The Langport Member-to-Blue Lias Formation transition, a previously debated flooding event (43, 44) corroborated here by the largest increase in the C_{30} sterane index (Fig. 2), is characterized by a negative shift in $\delta^{13}C_{org}$ and significant changes in biomarkers, including a switch from aerobic methanotrophy to cyanobacterial dominance and shifts in the proportions of C_{27} and C_{28} steranes (Fig. 2 and *SI Appendix*, Fig. S2). The base of the Blue Lias Formation is marked by microlaminated organic matter-rich mudstones ("paper shales"), the basal 2 cm of which contains a "Lilliput Assemblage" (45) of tiny (millimeter-scale) bivalves (*SI Appendix*, Fig. S4). The succeeding finely laminated paper shales and remaining Preplanorbis zone (lowermost Blue Lias Formation, lacking ammonites, specifically *Psiloceras planorbis*) are characterized by a pronounced positive $\delta^{13}C_{org}$ shift (Fig. 1) (4) and numerous levels of abundant completely decalcified and poorly preserved bivalves of low diversity (*SI Appendix*, Fig. S5), most simply interpreted as the results of a calcification crisis in which no aragonitic and few calcitic mollusks are preserved. Negative $\delta^{13}C_{org}$ values return with the reappearance of ammonites, particularly *P. planorbis* that preserve the aragonitic nacre (Fig. 1). A marked microfloral swing with an acme of the conifer pollen form *Classopollis meyeriana* also occurs at the base of the Blue Lias Formation. The appearance of *P. planorbis* along with the sporomorph taxon *Cerebropollenites thiergartii* within the extensive *C. meyeriana* acme marks the approximate base of the Hettangian (13). Previously interpreted as a product of another major disruption in the exchangeable reservoirs between the terrestrial and marine realms at the ETE (4), and used as a chemostratigraphic marker (main CIE), this negative shift is now recognized as a change to long-term relatively negative $\delta^{13}C_{org}$ values lasting through the Hettangian Age, rather than a single event (44, 46).

Compound-Specific Isotope Analysis of the CIE Supports Its Environmental Origin. Compound-specific isotope analysis (CSIA) of biomarkers provides insight into how ecological change(s) contribute to the values of the $\delta^{13}C_{org}$ record. Synchronous isotopic shifts of biomarkers at the CIE onset and termination generally allude to an exogenous ^{12}C source (Fig. 3 and *SI Appendix*, Fig. S6). However, the myriad variations in biomarker $\delta^{13}C$ values and the extent of excursions at the CIE between the two sections (Fig. 3 and *SI Appendix*, Table S1) do not support an exogenous ^{12}C source. Rather, the CIE reflects more complex endogenic origin(s) driven by ^{13}C-depleted carbon associated with microbial mats. Additionally, the low total organic-carbon contents throughout the CIE (<1%; typically 0.2%) imply that only relatively minor changes in organic-matter input would have pronounced significant effects on the $\delta^{13}C_{org}$ record. This section describes in more detail differences between values of various biomarker isotopes and the $\delta^{13}C_{org}$ record, as well as the complex array of sources and related processes affecting $\delta^{13}C_{org}$ values.

Biomarkers investigated by CSIA include pristane and phytane typically derived from chlorophylls *a* and *b* (cyanobacteria and/or algae) (47), $C_{17–19}$ *n*-alkanes from microbes including bacteria and algae (48), $C_{23–25}$ odd carbon-numbered *n*-alkanes from bryophytes (49) and other submergent plants (50, 51), and $>C_{25}$ odd carbon-numbered *n*-alkanes from land plants (52) (*SI Appendix*, Table S1).

Major differences in the biomarker $\delta^{13}C$ values observed between both sections occur at the onset of the CIE. For instance, at St. Audrie's Bay, phytane exhibits the largest isotopic shift (−5.1‰) that seemingly mirrors an equal shift in the bulk $\delta^{13}C_{org}$ record, whereas at Lilstock, the largest compound-specific isotopic shifts are recorded in the $C_{21–29}$ odd-numbered *n*-alkanes (−4.12 to −6.0‰), albeit lesser than the −8.1‰ bulk $\delta^{13}C_{org}$ excursion (Fig. 3 and *SI Appendix*, Fig. S6 and Table S1). In addition, during the termination of the CIE at Lilstock, some of the largest isotopic shifts occur in the $C_{21–29}$ odd-numbered *n*-alkanes with >5‰ positive shifts that are not mirrored in the bulk $\delta^{13}C_{org}$ record (3.6‰) (Fig. 3 and *SI Appendix*, Fig. S6 and Table S1). Such discrepancies exemplify the CIE reflects a more complex, endogenic origin related to ecological change(s).

The covariation of $\delta^{13}C_{org}$ and $\delta^{13}C_{phytane}$ values through the CIE indicates that the CIE can primarily be explained by microbial-community changes (Fig. 3). Specifically, within the CIE the most negative $\delta^{13}C_{org}$ values coincide with most negative $\delta^{13}C_{phytane}$ values (−34.8‰ and −33.9‰ at St. Audrie's Bay and Lilstock, respectively). Although pristane has its primary contributions from chlorophylls *a* and *b* in the water column, phytane has multiple predominant sources including cyanobacteria and methanogenic archaea residing in microbial mats as well as those from chlorophyll *a*- and *b*-containing photoautotrophic algae that reside in the water column. For example, phytane-related isoprenoids released after the cleavage of polar lipids have been detected in abundance in the hypersaline microbial mats of Shark Bay, Western Australia, and Laguna Guerrero Negro, Mexico (53, 54). Originating from archaeol, such compounds are indicative of methanogens found in a range of environments including microbial mats (55–57). In algae, *n*-alkyl lipids (e.g., $C_{17–19}$ *n*-alkanes) are depleted in ^{13}C compared to the cooccurring isoprenoids by ∼1.5‰, whereas in bacteria, the opposite pattern is observed (ref. 58 and references therein). Based on increases in heterotrophy given by the positive isotopic offsets between *n*-alkanes ($C_{17–19}$) and isoprenoids (pristane and phytane) and the ∼2‰ offsets between $\delta^{13}C_{pristane}$ and $\delta^{13}C_{phytane}$ during the CIE onset (Fig. 3), negative shifts in $\delta^{13}C_{phytane}$ are associated with increased bacterial activity of microbial mats. Enhanced preservation of phytane associated with microbial-mat formation explains low CIE pristane/phytane ratios, typically associated with more reducing conditions (59), during red-bed oxic deposition (*SI Appendix*, Fig. S2). Therefore, the incongruity of the interpretation of redox conditions based on lithologic observation and biomarkers suggests that the pristane/phytane ratio is a source indicator associated with microbial mats, rather than being simply an indicator of redox conditions (Fig. 2 and *SI Appendix*, Fig. S2).

Microbial mats are known to produce lipids with greater ^{13}C-depletion compared to those of phytoplankton (60). Investigations into the isotopic composition of phospholipid fatty acids in modern freshwater microbialites have shown lipids greatly depleted in ^{13}C ($\delta^{13}C$ values ranging between −31.4 ± 0.6 and 44.1 ± 0.5‰) (61, 62), and biomarkers of sulfate-reducing bacteria (important contributors in microbial-mat communities) in the carbonate matrix of concretions are also considerably ^{13}C-depleted ($\delta^{13}C$ values ranging between −40.5 and 42.0‰)

Downloaded at Columbia Univ Lib on January 14, 2021

(63). Furthermore, the recycling of ^{13}C-depleted autotrophic biomass by lower-residing heterotrophic layers within freshwater microbialites is required to explain changes in microbialite vertical $\delta^{13}C$ profiles and calcium carbonate precipitation equations whereby the local $\delta^{13}C_{DIC}$ becomes increasingly negative as a result of microbial respiration (64, 65). Thus, the ^{13}C-depleted organic carbon associated with freshwater microbial mats and respiration-induced release of ^{13}C-depleted carbon to the inorganic carbon pool and its reassimilation would be essential drivers of the CIE and possibly account for the minor offsets between the isotopic composition of pristane and phytane. Furthermore, methanogenic bacterial metabolism important in microbial mats produces methane in large quantities (37), meaning that microbial-mat emergence in the SW United Kingdom could constitute an important methane source unrelated to the CAMP.

In the same interval at Lilstock, odd-numbered mid- to long-chain *n*-alkanes ($C_{21–27}$) show isotopic values more depleted than those of phytane, ranging between −34.8 and −36.3‰ (*SI Appendix*, Table S1 and Fig. S6). The ^{13}C-depleted midchain-length *n*-alkanes may be attributed to bryophytes and possibly other submerged/floating plants, as corroborated by fossil evidence that includes the aquatic bryophyte (liverworts) *Naiadita* and *Hepaticites* (along with freshwater to brackish Crustacea) in the Cotham Member (7, 9). The ^{13}C-depletion of long-chain *n*-alkanes with odd over even preference within the CIE has been cited as evidence of an input of light carbon into the atmosphere (66), based on data from Austrian sections. These sections, while having an overall similar lithostratigraphy (Fig. 1) and similar patterns in *n*-alkanes differ from those of the BCB in having high total organic carbon (TOC) values in the CIE. Furthermore, the longer-chain *n*-alkane isotopic record fluctuates cyclically (67) through the St. Audrie's section (*SI Appendix*, Fig. S7), with more shifts in *n*-alkane than bulk organic $\delta^{13}C$, an observation more parsimoniously explained by episodic floral changes tied to cyclical climate rather than multiple changes in atmospheric composition. Pollen and spore data from St. Audrie's Bay track mid- to long-chain *n*-alkane isotope values (Fig. 3 and *SI Appendix*, Fig. S6 and Table S1) through the CIE (13). The CIE onset closely correlates with a greater abundance of pollen (dominated by *C. meyeriana*) and terminates with a greater abundance of spores, the largest turnover in sporomorph taxa (Fig. 3). Spore-bearing plants such as lycophytes and monilophytes can exhibit higher carbon isotopic discrimination compared to pollen-bearing plants (e.g., gymnosperm and angiosperm) by up to ∼5‰ in $\delta^{13}C$ values (68). Variation in plant inputs, although unlikely being the primary explanation of the CIE, most possibly is a consequence of local hydrologic/climatic shifts amplifying isotopic shifts and contributing to the CIE (69). The shifts between autotrophic algae vs. heterotrophic bacteria together with cyclical land plant inputs (58, 70) during the CIE explain geochemical variations and differences, highlighting that local environmental changes triggered the onset and termination of the CIE, supporting that the CIE is endogenic in its origin.

Following the CIE, the $\delta^{13}C$ of pristane and phytane in the middle Langport Member are relatively constant, and phytane is interpreted as being sourced largely from chlorophylls *a* and *b*. $\delta^{13}C$ values of the C_{17} to C_{19} and C_{29} *n*-alkanes are generally more positive, with the exception of one negative excursion that has a negligible effect on the $\delta^{13}C_{org}$ record and is coincident with pollen and spore changes and heavy bioturbation. Above this, across the upper Langport-to-Blue Lias transition, the $\delta^{13}C$ of pristane and phytane become relatively less stable, particularly at St. Audrie's Bay, and all *n*-alkanes, particularly C_{19} and C_{29}, show a negative excursion coincident with increases in *Classopollis* pollen and a negative shift in the $\delta^{13}C_{org}$ record (Fig. 3).

Revised Relationship between the CIE and ETE. At the end-Triassic, extinction and isotopic events in multiple sections across Europe occur in different orders. In the BCB, the floral change occurs at the CIE prior to the last appearance of conodonts, whereas in the Austrian sections, the floral changes occur after the CIE and the last appearance of conodonts (Fig. 1). Correlations between the last occurrence of conodont taxa in the United Kingdom and conodont extinction of the same taxa in Austrian sections suggest the lowermost Blue Lias Formation correlates to the *Choristoceras marshi* ammonite zone, which is largely regarded as occurring at the base of the marine-extinction level (71). Recent work placed the UK marine extinction in the "dead zone" of the upper Cotham Member (10); however, this dead zone simply lacks marine invertebrates because it is a nonmarine environment subjected to desiccation. The subsequent appearance of conodonts with the return of marine conditions suggests instead that the marine extinction level is at the base of the Blue Lias Formation. Here, the last phytosaurs (42) and conodonts (12), and low-diversity, poorly preserved and decalcified marine taxa are due to one or more abrupt large increases in P_{CO_2} of CAMP origin. The negative $\delta^{13}C_{org}$ excursion at this level and the overlying positive $\delta^{13}C_{org}$ excursion might be a globally correlative marker (Fig. 1), more directly connected to exogenous carbon isotopic shifts related to the CAMP. This hypothesis may resolve the long-standing nonunique correlations deploying the CIE as the key event (67, 72, 73).

Biomarker and isotope data support the hypothesis that the CIE was caused by regional phenomena related to shallow-water microbial mats in a transient freshwater to brackish setting, as summarized in Fig. 4, rather than the CAMP-induced release of ^{13}C-depleted gasses such as methane. The organic carbon cycle changed in complex ways, with the CIE reflecting temporally, and to a lesser extent geographically, varying ecological changes, with concomitant isotopic shifts of differing magnitudes deposited during an interval of intense environmental change. By this hypothesis, the CIE was driven by microbial-community changes and mat emergence because of regional relative sea-level fall and a shift from restricted marine to nonmarine environments. Therefore, global chemostratigraphic correlations between the SW United Kingdom and other globally distributed sections must be revised. Many studied ETE sections with $\delta^{13}C_{org}$ records are from shallow marine to coastal environments in central European basins. As such, they too are potentially influenced by changing salinity and water depth. For example, in the Eiberg Basin, Austria, increases in the freshwater alga *Botryococcus* during the CIE may be responsible for the large negative-isotopic excursion in long-chain *n*-alkanes (74). It is noteworthy that in in fully continental sections, where $\delta^{13}C$ can be traced in the cuticle lipids of specific plant taxa, a negative CIE is not observed at the base of the extinction level (75).

The origin of the regional abrupt sea-level drop that allowed the development of shallow freshwater-microbial mats at the CIE may be tied to the onset phase of the CAMP, which is now known to begin before the ETE (2). Plausible specific mechanisms include 1) rising of hot asthenosphere causing doming of the crust and uplift of the European basins (76) or closure of marine gateways into the already restricted European basins, either or both of which would be predicted to cause transient sea level rise elsewhere; and 2) eustatic sea-level drop if initiation of CAMP volcanism involved sustained SO_2 emissions, which could have led to the transient growth of glaciers (77). These hypotheses are consistent with our observations in the Bristol Channel and European basins. Confirmation must be sought through future ETE-biomarker and compound-specific isotopic investigations in pelagic sequences that are not affected by changes in salinity and water depth, such as at Katsuyama, Japan (78), but that also have independent means of

Downloaded at Columbia Univ Lib on January 14, 2021

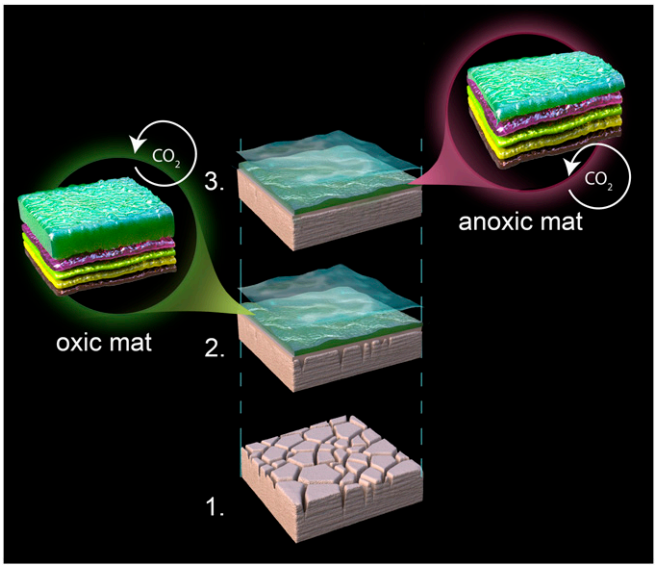

Fig. 4. Development of a microbial mat in the BCB at the time of the terminal Triassic CIE: sea-level regression resulting in subareal exposure and desiccation of the seabed, initiating the CIE (1); formation of an oxic microbial mat with abundant cyanobacteria (oxygenic photosynthetic bacteria) under shallow, fresh to brackish water (2); and transition to an anoxic microbial mat with abundant Chromatiaceae (obligate anoxygenic phototrophic purple sulfur bacteria) and green pigmented Chlorobi (strict anoxygenic phototrophic green sulfur bacteria) (3). Circular arrows in 2 and 3 indicate microbial mat-induced recycling of CO_2 and resultant ^{12}C enrichment.

correlation such as magnetostratigraphy, U-Pb geochronology, and astrochronology.

Conclusions

Biomarker and compound-specific isotopic data from the BCB at St. Audrie's Bay and Lilstock, United Kingdom, show that the iconic CIE preceded the main ETE and that the CIE itself is a record of freshwater microbial-mat development and other ecological changes driven by a geologically transient, regional sea-level change. Use of the BCB CIE and its European correlates as a global isochronous chemostratigraphic marker is therefore not tenable. The succeeding smaller negative-isotopic excursion at the onset of the biocalcification event, associated with the last conodonts and the last phytosaurs, might be such a global isochronous marker. This interpretation of the CIE requires a reanalysis of global correlations at a tens of thousands of years resolution with independent correlation methods and should lead to a better understanding of the regional vs. global effects of the CAMP on one of the largest mass extinctions in Earth's history.

Materials and Methods

For $\delta^{13}C_{org}$ and TOC analyses, carbonates were removed from samples (dry weight, <0.5 g) by acid digestion and measured using a Delta V Plus mass spectrometer connected to a Thermo Flash 1112 via a Conflo IV and a carbon, hydrogen, nitrogen, and sulfur elemental analyzer at the West Australian Biogeochemistry Centre, University of Western Australia. For biomarker analysis, bitumens were isolated from dry-sediment samples (30 to 180 g) by solvent extraction using a Milestone Start-E microwave extraction system in 50 mL of 9:1 dichloromethane:methanol (DCM:MeOH) using a temperature program of 21 to 80 °C over 10 min (held for 15 min). Elemental sulfur was removed using activated copper turnings, and bitumen compounds were separated into saturate (*n*-hexane), aromatic (3:1 *n*-hexane:DCM), and polar (9:1 DCM:MeOH) fractions using column chromatography with activated silica gel. St. Audrie's Bay saturate fractions were analyzed using an Agilent 6890N gas chromatograph (GC) connected to a Micromass AutoSpec Ultima multiple reaction-monitoring mass spectrometer (MRM-MS). St. Audrie's Bay aromatic and Lilstock combined saturate and aromatic fractions were analyzed using an Agilent 7890B GC connected to an Agilent 7010A triple quadrupole (QQQ) tandem MS. All GC-MRM-MS and GC-QQQ-MS analyses were conducted at R.E.S.'s laboratory, Massachusetts Institute of Technology. Details on quality control regarding multiple-instrument measurements are expanded in *SI Appendix*. Compound-specific isotope analysis was conducted at Curtin University using a Thermo Trace GC Ultra connected to a Thermo Delta V Advantage isotope-ratios MS via a GC Isolink and Conflo IV. For full materials and methods, see *SI Appendix*.

Data Availability. All study data are included in the article and supporting information.

ACKNOWLEDGMENTS. We acknowledge Peter Hopper, Alex Holman, and P. Sargent Bray for technical support and Victor Leshyk for schematics. C.P.F. acknowledges Curtin University for an international scholarship (this paper forms a fundamental chapter of C.P.F.'s thesis). C.P.F. (PhD scholarship) and K.G. (funding for Triassic/Jurassic) acknowledge the Australian Research Council (ARC) for Linkage funding (Grant LP150100341) supporting this work. K.G. acknowledges the ARC for three infrastructure grants for CSIA (Grant LE110100119) and bulk isotope work (Grants LE100100041 and LE0882836). C.P.F. acknowledges the European Association of Organic Geochemistry for a travel scholarship award. J.H.W. and R.E.S. acknowledge support from NSF Grant EAR 1147402. X.C. and R.E.S. acknowledge the Simons Foundation Collaboration on the Origins of Life (Grant 290361FY18). P.E.O. acknowledges fieldwork support from the Lamont Climate Center. C.P.F. also acknowledges Khalifa University of Science and Technology (Grant CIRA-2019-066). We are grateful to Bob Cornes of Natural England for permission to sample the foreshore in Somerset and guidance for sampling permission from the Orchard-Wyndham estate. We thank reviewers Simon George and Jennifer McElwain for their constructive comments, which helped significantly improve this manuscript. This is Lamont-Doherty Earth Observatory contribution 8454.

1. D. H. Rothman, Thresholds of catastrophe in the Earth system. *Sci. Adv.* **3**, e1700906 (2017).
2. J. Davies *et al.*, End-Triassic mass extinction started by intrusive CAMP activity. *Nat. Commun.* **8**, 15596 (2017).
3. T. J. Blackburn *et al.*, Zircon U-Pb geochronology links the end-Triassic extinction with the central atlantic magmatic province. *Science* **340**, 941–945 (2013).
4. S. P. Hesselbo, S. A. Robinson, F. Surlyk, S. Piasecki, Terrestrial and marine extinction at the Triassic-Jurassic boundary synchronized with major carbon-cycle perturbation: A link to initiation of massive volcanism? *Geology* **30**, 251–254 (2002).
5. M. Ruhl, W. M. Kürschner, L. Krystyn, Triassic–Jurassic organic carbon isotope stratigraphy of key sections in the western Tethys realm (Austria). *Earth Planet. Sci. Lett.* **281**, 169–187 (2009).
6. A. von Hillebrandt *et al.*, The global stratotype sections and point (GSSP) for the base of the Jurassic system at Kuhjoch (Karwendel Mountains, Northern Calcareous Alps, Tyrol, Austria). *Episodes* **36**, 162–198 (2013).
7. M. Mayall, An earthquake origin for synsedimentary deformation in a late Triassic (Rhaetian) lagoonal sequence, southwest Britain. *Geol. Mag.* **120**, 613–622 (1983).
8. W. S. Lacey, Fossil bryophytes. *Biol. Rev. Camb. Philos. Soc.* **44**, 189–205 (1969).
9. E. Poole, The Triassic-Jurassic boundary in great Britain. *Geol. Mag.* **116**, 303–311 (1979).
10. L. Mander, R. J. Twitchett, M. J. Benton, Palaeoecology of the Late Triassic extinction event in the SW UK. *J. Geol. Soc. London* **165**, 319–332 (2008).
11. P. B. Wignall, D. P. G. Bond, The end-Triassic and Early Jurassic mass extinction records in the British Isles. *Proc. Geolog. Assoc.* **119**, 73–84 (2008).
12. A. Swift, First records of conodonts from the Late Triassic of Britain. *Palaeontology* **32**, 325–333 (1989).
13. N. R. Bonis, M. Ruhl, W. M. Kürschner, Milankovitch-scale palynological turnover across the Triassic–Jurassic transition at St. Audrie's Bay, SW UK. *J. Geol. Soc. London* **167**, 877–888 (2010).
14. A. Swift, "Stratigraphy (including biostratigraphy)" in *Fossils of the Rhaetian Penarth Group, Field Guides to Fossils 9*, A. Swift, D.J. Martill, Eds. (Palaeontological Association, London, 1999), pp. 15–30.
15. A. Hallam, The case for sea-level change as a dominant causal factor in mass extinction of marine invertebrates. *Philos. Trans. R. Soc. Lond. B Biol. Sci.* **325**, 437–455 (1989).
16. M. J. Simms, Uniquely extensive soft-sediment deformation in the Rhaetian of the UK: Evidence for earthquake or impact? *Palaeogeogr. Palaeoclimatol. Palaeoecol.* **244**, 407–423 (2007).
17. H. C. Ivimey-Cook, "The Permian and Triassic deposits of wales" in *The Upper Palaeozoic and Post-Palaeozoic Rocks of Wales*, T. R. Owen, Ed. (University of Wales Press, Cardiff, 1974), pp. 295–321.

Downloaded at Columbia Univ Lib on January 14, 2021

18. J. S. Sinninghe Damsté *et al*., Evidence for gammacerane as an indicator of water column stratification. *Geochim. Cosmochim. Acta* **59**, 1895–1900 (1995).
19. J. A. Maresca, S. P. Romberger, D. A. Bryant, Isorenieratene biosynthesis in green sulfur bacteria requires the cooperative actions of two carotenoid cyclases. *J. Bacteriol.* **190**, 6384–6391 (2008).
20. R. E. Summons, T. G. Powell, Chlorobiaceae in Palaeozoic seas revealed by biological markers, isotopes and geology. *Nature* **319**, 763–765 (1986).
21. K. Grice, P. Schaeffer, L. Schwark, J. R. Maxwell, Molecular indicators of palaeoenvironmental conditions in an immature Permian shale (Kupferschiefer, Lower Rhine Basin, north-west Germany) from free and S-bound lipids. *Org. Geochem.* **25**, 131–147 (1996).
22. K. Grice, P. Schaeffer, L. Schwark, J. R. Maxwell, Changes in palaeoenvironmental conditions during deposition of the Permian Kupferschiefer (Lower Rhine Basin, northwest Germany) inferred from molecular and isotopic compositions of biomarker components. *Org. Geochem.* **26**, 677–690 (1997).
23. S. E. Rashby, A. L. Sessions, R. E. Summons, D. K. Newman, Biosynthesis of 2-methylbacteriohopanepolyols by an anoxygenic phototroph. *Proc. Natl. Acad. Sci. U.S.A.* **104**, 15099–15104 (2007).
24. J. Ricci, A. Michel, D. Newman, Phylogenetic analysis of HpnP reveals the origin of 2-methylhopanoid production in Alphaproteobacteria. *Geobiology* **13**, 267–277 (2015).
25. J. N. Ricci *et al*., Diverse capacity for 2-methylhopanoid production correlates with a specific ecological niche. *ISME J.* **8**, 675–684 (2014).
26. J. Ricci, R. Morton, G. Kulkarni, M. Summers, D. Newman, Hopanoids play a role in stress tolerance and nutrient storage in the cyanobacterium Nostoc punctiforme. *Geobiology* **15**, 173–183 (2017).
27. T. J. Garby, M. R. Walter, A. W. Larkum, B. A. Neilan, Diversity of cyanobacterial biomarker genes from the stromatolites of Shark Bay, Western Australia. *Environ. Microbiol.* **15**, 1464–1475 (2013).
28. J. J. Brocks, P. Schaeffer, Okenane, a biomarker for purple sulfur bacteria (Chromatiaceae), and other new carotenoid derivatives from the 1640 Ma Barney Creek Formation. *Geochim. Cosmochim. Acta* **72**, 1396–1414 (2008).
29. K. French, D. Rocher, J. Zumberge, R. Summons, Assessing the distribution of sedimentary C 40 carotenoids through time. *Geobiology* **13**, 139–151 (2015).
30. S. L. Jensen, Bacterial carotenoids. *Acta Chem. Scand.* **19**, 1025–1030 (1965).
31. J. E. Graham, D. A. Bryant, The biosynthetic pathway for synechoxanthin, an aromatic carotenoid synthesized by the euryhaline, unicellular cyanobacterium Synechococcus sp. strain PCC 7002. *J. Bacteriol.* **190**, 7966–7974 (2008).
32. J. E. Graham, J. T. Lecomte, D. A. Bryant, Synechoxanthin, an aromatic C40 xanthophyll that is a major carotenoid in the cyanobacterium Synechococcus sp. PCC 7002. *Journal of natural products* **71**, 1647–1650 (2008).
33. X. Cui *et al*., Niche expansion for phototrophic sulfur bacteria at the Proterozoic–Phanerozoic transition. *Proc. Natl. Acad. Sci. U.S.A.* **117**, 17599–17606 (2020).
34. G. Kleemann *et al*., Tetrahymanol from the phototrophic bacterium Rhodopseudomonas palustris: First report of a gammacerane triterpene from a prokaryote. *Microbiology* **136**, 2551–2553 (1990).
35. F. B. Mallory, J. T. Gordon, R. L. Conner, The isolation of a pentacyclic triterpenoid alcohol from a protozoan. *J. Am. Chem. Soc.* **85**, 1362–1363 (1963).
36. C. Neubauer *et al*., Lipid remodeling in Rhodopseudomonas palustris TIE-1 upon loss of hopanoids and hopanoid methylation. *Geobiology* **13**, 443–453 (2015).
37. C. M. Prieto-Barajas, E. Valencia-Cantero, G. Santoyo, Microbial mat ecosystems: Structure types, functional diversity, and biotechnological application. *Electron. J. Biotechnol.* **31**, 48–56 (2018).
38. Y. Ibarra, F. A. Corsetti, S. E. Greene, D. J. Bottjer, Microfacies of the Cotham marble: A tubestone carbonate microbialite from the Upper Triassic, southwestern UK. *Palaios* **29**, 1–15 (2014).
39. Y. Ibarra, F. A. Corsetti, S. E. Greene, D. J. Bottjer, A microbial carbonate response in synchrony with the end-Triassic mass extinction across the SW UK. *Sci. Rep.* **6**, 19808 (2016).
40. B. Schaefer *et al*., Microbial life in the nascent Chicxulub crater. *Geology* **48**, 328–332 (2020).
41. K. L. French, J. E. Birdwell, M. V. Berg, Biomarker similarities between the saline lacustrine eocene green river and the paleoproterozoic barney creek formations. *Geochim. Cosmochim. Acta* **274**, 228–245 (2020).
42. M. W. Maisch, M. Kapitzke, A presumably marine phytosaur (Reptilia: Archosauria) from the pre-planorbis beds (Hettangian) of England. *Neues Jahrb. Geol. Paläontol. Abh.* **257**, 373–379 (2010).
43. T. Hallam, P. Wignall, S. P. Hesselbo, S. A. Robinson, F. Surlyk, Discussion on sea-level change and facies development across potential Triassic–Jurassic boundary horizons, SW Britain. *J. Geol. Soc. London* **161**, 1053–1056 (2004).
44. S. P. Hesselbo, S. A. Robinson, F. Surlyk, Sea-level change and facies development across potential Triassic–Jurassic boundary horizons, SW Britain. *J. Geol. Soc. London* **161**, 365–379 (2004).
45. A. Urbanek, Biotic crises in the history of upper silurian graptoloids: A palaeobiological model. *Hist. Biol.* **7**, 29–50 (1993).
46. M. Ruhl *et al*., Astronomical constraints on the duration of the early Jurassic Hettangian stage and recovery rates following the end-Triassic mass extinction (St Audrie's Bay/East Quantoxhead, UK). *Earth Planet. Sci. Lett.* **295**, 262–276 (2010).
47. T. Powell, D. McKirdy, Relationship between ratio of pristane to phytane, crude oil composition and geological environment in Australia. *Nat. Phys. Sci (Lond.)* **243**, 37–39 (1973).
48. P. Cranwell, G. Eglinton, N. Robinson, Lipids of aquatic organisms as potential contributors to lacustrine sediments—II. *Org. Geochem.* **11**, 513–527 (1987).
49. M. Baas, R. Pancost, B. van Geel, J. S. S. Damsté, A comparative study of lipids in Sphagnum species. *Org. Geochem.* **31**, 535–541 (2000).
50. K. J. Ficken, B. Li, D. Swain, G. Eglinton, An n-alkane proxy for the sedimentary input of submerged/floating freshwater aquatic macrophytes. *Org. Geochem.* **31**, 745–749 (2000).
51. S. Tulipani, K. Grice, E. Krull, P. Greenwood, A. T. Revill, Salinity variations in the northern Coorong Lagoon, South Australia: Significant changes in the ecosystem following human alteration to the natural water regime. *Org. Geochem.* **75**, 74–86 (2014).
52. G. Eglinton, A. Gonzalez, R. Hamilton, R. Raphael, Hydrocarbon constituents of the wax coatings of plant leaves: A taxonomic survey. *Phytochemistry* **1**, 89–102 (1962).
53. M. A. Allen, B. A. Neilan, B. P. Burns, L. L. Jahnke, R. E. Summons, Lipid biomarkers in Hamelin Pool microbial mats and stromatolites. *Org. Geochem.* **41**, 1207–1218 (2010).
54. L. Jahnke *et al*., Lipid biomarker and phylogenetic analyses to reveal archaeal biodiversity and distribution in hypersaline microbial mat and underlying sediment. *Geobiology* **6**, 394–410 (2008).
55. K. L. Lim, R. D. Pancost, E. R. Hornibrook, P. J. Maxfield, R. P. Evershed, Archaeol: An indicator of methanogenesis in water-saturated soils. *Archaea* **2012**, 896727 (2012).
56. R. D. Pancost *et al*., Archaeol as a methanogen biomarker in ombrotrophic bogs. *Org. Geochem.* **42**, 1279–1287 (2011).
57. M. Sunamura, Y. Koga, K. Ohwada, Biomass measurement of methanogens in the sediments of Tokyo Bay using archaeol lipids. *Mar. Biotechnol. (NY)* **1**, 562–568 (1999).
58. K. Grice *et al*., Photic zone euxinia during the Permian-Triassic superanoxic event. *Science* **307**, 706–709 (2005).
59. B. Didyk, B. Simoneit, S. t. Brassell, G. Eglinton, Organic geochemical indicators of palaeoenvironmental conditions of sedimentation. *Nature* **272**, 216–222 (1978).
60. G. A. Logan *et al*., Terminal Proterozoic mid-shelf benthic microbial mats in the Centralian Superbasin and their environmental significance. *Geochim. Cosmochim. Acta* **63**, 1345–1358 (1999).
61. A. Brady *et al*., Photosynthetic isotope biosignatures in laminated micro-stromatolitic and non-laminated nodules associated with modern, freshwater microbialites in Pavilion Lake, BC. *Chem. Geol.* **274**, 56–67 (2010).
62. R. A. White *et al*., Biosignatures associated with freshwater microbialites. *Life* **10**, 66 (2020).
63. I. Melendez *et al*., Biomarkers reveal the role of photic zone euxinia in exceptional fossil preservation: An organic geochemical perspective. *Geology* **41**, 123–126 (2013).
64. M. Breitbart *et al*., Metagenomic and stable isotopic analyses of modern freshwater microbialites in Cuatro Ciénegas, Mexico. *Environ. Microbiol.* **11**, 16–34 (2009).
65. A. Nitti *et al*., Spatially resolved genomic, stable isotopic, and lipid analyses of a modern freshwater microbialite from Cuatro Ciénegas, Mexico. *Astrobiology* **12**, 685–698 (2012).
66. M. Ruhl, N. R. Bonis, G.-J. Reichart, J. S. S. Damsté, W. M. Kürschner, Atmospheric carbon injection linked to end-Triassic mass extinction. *Science* **333**, 430–434 (2011).
67. J. H. Whiteside, P. E. Olsen, T. Eglinton, M. E. Brookfield, R. N. Sambrotto, Compound-specific carbon isotopes from Earth's largest flood basalt eruptions directly linked to the end-Triassic mass extinction. *Proc. Natl. Acad. Sci. U.S.A.* **107**, 6721–6725 (2010).
68. A. S. Porter, C. Yiotis, I. P. Montañez, J. C. McElwain, Evolutionary differences in Δ13C detected between spore and seed bearing plants following exposure to a range of atmospheric O2: CO2 ratios; implications for paleoatmosphere reconstruction. *Geochim. Cosmochim. Acta* **213**, 517–533 (2017).
69. K. H. Williford, K. Grice, A. Holman, J. C. McElwain, An organic record of terrestrial ecosystem collapse and recovery at the Triassic–Jurassic boundary in East Greenland. *Geochim. Cosmochim. Acta* **127**, 251–263 (2014).
70. C. M. Jaraula *et al*., Elevated pCO2 leading to Late Triassic extinction, persistent photic zone euxinia, and rising sea levels. *Geology* **41**, 955–958 (2013).
71. C. A. McRoberts, L. Krystyn, M. Hautmann, Macrofaunal response to the end-Triassic mass extinction in the West-Tethyan Kössen Basin, Austria. *Palaios* **27**, 607–616 (2012).
72. S. Lindström *et al*., A new correlation of Triassic–Jurassic boundary successions in NW Europe, Nevada and Peru, and the Central Atlantic magmatic province: A time-line for the end-Triassic mass extinction. *Palaeogeogr. Palaeoclimatol. Palaeoecol.* **478**, 80–102 (2017).
73. J. A. Yager *et al*., Duration of and decoupling between carbon isotope excursions during the end-Triassic mass extinction and Central Atlantic Magmatic Province emplacement. *Earth Planet. Sci. Lett.* **473**, 227–236 (2017).
74. A. Bachan, B. van de Schootbrugge, J. L. Payne, The end-Triassic negative δ13C excursion: A lithologic test. *Palaeogeogr. Palaeoclimatol. Palaeoecol.* **412**, 177–186 (2014).
75. K. L. Bacon, C. M. Belcher, S. P. Hesselbo, J. C. McElwain, The Triassic-Jurassic boundary carbon-isotope excursions expressed in taxonomically identified leaf cuticles. *Palaios* **26**, 461–469 (2011).
76. A. Hallam, Z. E. Shaarawy, Salinity reduction of the end-Triassic sea from the Alpine region into northwestern Europe. *Lethaia* **15**, 169–178 (1982).
77. B. Schoene, J. Guex, A. Bartolini, U. Schaltegger, T. J. Blackburn, Correlating the end-Triassic mass extinction and flood basalt volcanism at the 100 ka level. *Geology* **38**, 387–390 (2010).
78. W. Fujisaki *et al*., Global perturbations of carbon cycle during the Triassic–Jurassic transition recorded in the mid-Panthalassa. *Earth Planet. Sci. Lett.* **500**, 105–116 (2018).

Downloaded at Columbia Univ Lib on January 14, 2021